RAMP-EDGE JOSEPHSON JUNCTIONS BASED ON ELECTRON-DOPED CUPRATES

BY PATRICK FOURNIER, SOPHIE CHARPENTIER, GUILLAUME ROBERGE, SÉBASTIEN GODIN-PROULX

SUMMARY

We present a quick survey of the properties of Josephson junctions and a few strategies used to fabricate them with cuprate high temperature superconductors. As an example, we show our recent results on ramp-edge junctions where both superconducting electrodes and the barrier are based on electron-doped cuprates. These superconducting-normal-superconducting junctions obtained in the ramp-edge geometry present current-voltage characteristics, field dependence of the critical current and Shapiro steps in ambient RF field confirming their quality. They can be used to study the proximity effect through electron-doped barriers with different doping levels.

JOSEPHSON EFFECT AND HIGH T_C JUNCTIONS

Many of the interesting applications of superconductivity rely on the possibility to couple the phase of the macroscopic wave-functions of two superconducting electrodes separated by a non-superconducting barrier. This phenomenon, called the Josephson Effect, leads to devices that behave essentially like weak superconducting links with pairs tunnelling coherently through the barrier [1]. Assuming macroscopic pair wave-functions $\psi_L = \rho_L^{1/2} e^{i\theta_L}$ and $\psi_R = \rho_R^{1/2} e^{i\theta_R}$ for the left (L) and right (R)-side electrodes respectively (here ρ_i and θ_i are the superfluid density and the phase of the respective electrodes, i = R or L), one can use the following Schrödinger equations to the lowest (linear) order in coupling to describe the behaviour of these wave-functions on each side of the barrier:

$$i\hbar\frac{\partial\Psi_L}{\partial t} = E_L\Psi_L + K\Psi_R \text{ and } i\hbar\frac{\partial\Psi_R}{\partial t} = E_R\Psi_R + K\Psi_L \quad (1)$$

where E_L and E_R are the ground state energies of the Cooper pairs in the isolated superconducting electrodes and K is the coupling constant of the interaction term proportional to the "leaking" wave-function of the nearby electrode. In the general case when a potential difference V is applied between the two superconducting banks, one gets $E_L - E_R = -2eV$ resulting from Eq. (1) in four separate equations for the time dependence of the phases and the superfluid densities:

$$\frac{\partial\phi_R}{\partial t} = -\frac{K}{\hbar}\left(\frac{\rho_L}{\rho_R}\right)\cos\gamma + \frac{eV}{\hbar} \quad (2)$$

$$\frac{\partial\phi_L}{\partial t} = -\frac{K}{\hbar}\left(\frac{\rho_R}{\rho_L}\right)\cos\gamma - \frac{eV}{\hbar} \quad (3)$$

$$\frac{\partial\rho_R}{\partial t} = -\frac{2K}{\hbar}(\rho_L\rho_R)^{1/2}\sin\gamma \quad (4)$$

$$\frac{\partial\rho_L}{\partial t} = \frac{2K}{\hbar}(\rho_L\rho_R)^{1/2}\sin\gamma \quad (5)$$

where $\gamma \equiv \theta_R - \theta_L$ is the phase difference between the electrodes. Since the current density flowing through the junction as a part of a closed circuit is naturally related to the variation in time of the superfluid density, i.e. $J = -2e\frac{\partial\rho_R}{\partial t}$, one obtains:

$$J = J_0\sin\gamma \quad (6)$$

where J_0 depends on K, ρ_R and ρ_L. Thus, the current flowing between the superconducting electrodes is set by the difference in the phase $\gamma \equiv \theta_R - \theta_L$ of the wave-functions on each side of the junctions. External DC magnetic and AC electric fields can influence this phase difference (as shown in Eqs. 2 and 3) leading to spectacular behaviours exploited for example in the most sensitive magnetic field detector, the superconducting quantum interference device (SQUID) [2].

Josephson junctions based on high temperature superconductors (HTSC) are of obvious interest since they can be integrated in devices operating at high temperatures, not really available for conventional superconductors. High temperature SQUIDs based on HTSC and used at 77K in liquid nitrogen have been implemented for the detection of small magnetic fields produced by objects maintained at room temperature [3]. They are also of interest for fundamental research as their sensitivity to the phase of the superconducting order parameter (see Eqs. 2 – 5) can be used to probe the

P. Fournier <Patrick.Fournier@USherbrooke.ca>, Regroupement Québécois sur les Matériaux de Pointe, Institut Trans-disciplinaire en Information Quantique; Département de physique, Université de Sherbrooke, Sherbrooke, QC, J1K 2R1; et membre du programme Matériaux quantiques, Institut canadien de recherches avancées, Toronto, ON, M5G 1Z8

S. Charpentier, G. Roberge, S. Godin-Proulx, Département de physique, Université de Sherbrooke, Sherbrooke, QC, J1K 2R1

presence of unconventional superconductivity: for HTSC, a variety of junctions and SQUIDs were used to confirm the d-wave symmetry of their order parameter [4,5].

Obviously, fabricating junctions presenting controlled properties with a good yield remains a challenge with complex oxide materials that are usually very sensitive to *corrosive* environments. The resulting structural and impurity defects in proximity to or at the interfaces between the barrier and the electrodes are extremely difficult to fully control. Very successful approaches (strategies) to fabricate Josephson junctions with cuprates, mostly established using $YBa_2Cu_3O_7$ (YBCO), were proposed over the years in order to circumvent these difficulties [6]. In Figure 1, we show schematics of the most popular cuprate devices fabricated and studied. They are: (a) the bicrystal junction which takes advantage of the disrupted thin film growth above the grain boundary between two fused single crystals with tilted in-plane lattice parameters; (b) the bi-epitaxial junction resulting from the growth of a thin film with different orientations directly onto the substrate and on a seed layer; (c) the step-edge junction requiring the fabrication of a step or a ramp etched on the surface of a substrate prior to the deposition of the film; and finally (d) the ramp-edge junction where a ramp is fabricated out of a first bottom superconducting (SC) electrode, and then a second deposition run is used to obtain the barrier and the *top* SC electrode (see Ref. [6] for more details).

ALL-ELECTRON-DOPED JUNCTIONS

To give a better perspective of the typical steps involved in the fabrication of cuprate-based Josephson junctions, we focus in the following on the fabrication and properties of ramp-edge junctions with electron-doped cuprates, a family of HTSC renown for their difficult growth. In Figure 2, we present this configuration as an inset: in such device, the tunnelling current between the superconducting electrodes flows parallel to the surface of the substrate and along the copper-oxygen (CuO_2) planes of the crystal structure. Successful fabrication of such ramp-edge junctions were reported for several hole-doped cuprates [6] like $YBa_2Cu_3O_7$ and $La_{2-x}Sr_xCuO_4$, but little has been done with electron-doped cuprates of general formula $R_{2-x}Ce_xCuO_4$ (R = Pr, Nd, Sm,...). Our results demonstrate the high quality of our "all-electron-doped cuprate" junctions in which the barrier is a non-superconducting electron-doped cuprate.

In order to obtain the device shown in the inset of Fig. 1, several steps of growth and fabrication are required [7]. In summary, thin films of epitaxial $Pr_{2-x}Ce_xCuO_4$ (PCCO) with x = 0.15 and amorphous $SrTiO_3$ (STO-A) are grown by pulsed-laser deposition (PLD) on $5\times5mm^2$ $(LaAlO_3)_{0.3}$-$(Sr_2AlTaO_6)_{0.7}$ (LSAT) or $SrTiO_3$ (STO) (001) [8]. A ramp through the top STO-A and the bottom PCCO layers down to the substrate across the whole bilayer is defined by Ar ion milling. This process produces ramps at angles of roughly 30° with respect to the surface of the substrates as measured using atomic force microscopy. Following this milling process, a second PLD growth run for the non-superconducting PCCO barrier with x = 0.05 and the superconducting counter-electrode (with x = 0.15) follows immediately. Barrier thicknesses along the tunnelling direction (along the CuO_2 planes of the electrodes) varying from 5 to 50 nm were explored. Because additional fabrication steps based on ion

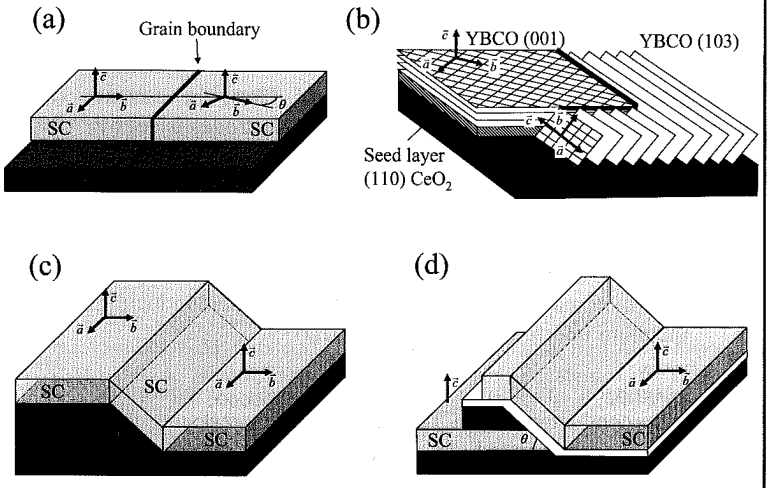

Fig. 1 Schematics of different strategies for the fabrication of Josephson junctions based on HTSC. They are: (a) the bicrystal, (b) the bi-epitaxial, (c) the step-edge and (d) the ramp-edge geometries. Arrows indicate the crystal axes of the films. Except for (b), the gray layers are superconducting (SC), the black and the white layers in (d) are respectively an insulator and the barrier. Inspired from Ref. [6].

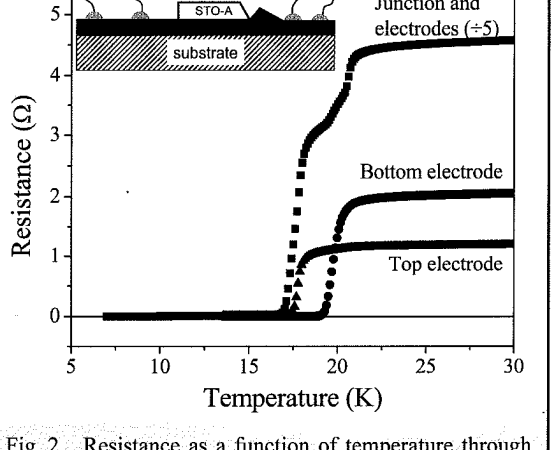

Fig. 2 Resistance as a function of temperature through the barrier (squares), in the top electrode (circles) and in the bottom electrode (triangles). Inset: schematic of the ramp-edge junctions. In dark grey, the superconducting PCCO x = 0.15 electrodes. In black, the non-superconducting PCCO x = 0.05 barrier. In white, the amorphous $SrTiO_3$ (STO-A) layer. Contacts and wires are also shown for the measurements through the barrier. Sketch not to scale.

milling to define narrow bridges of a few tens of microns were found to deteriorate the ramp-edge junctions, narrow bridges were made manually with a fine diamond scriber. Each sample of 5×5mm^2 could contain up to five junctions with widths varying from 50 to 200 μm and could be measured all at once at low temperature. IV curve measurements as a function of temperature and magnetic field were carried out in a shielded cryostat with a remnant ambient field of roughly 0.5 mG. Shapiro steps were obtained in the presence of a RF field transmitted to the sample via a separated coaxial transmission line ending with an antenna just above the sample.

In Figure 2, we present the resistance as a function of temperature in three different configurations. Two of them probe separately the resistance of the electrodes. We can observe a slight difference in their values of T_c likely due to the prolonged in-situ reduction time of the bottom electrode with respect to the top one: it was actually submitted to two reduction processes. This figure shows also the resistance of the sample through the barrier with the expected double transition as it reached zero resistance at the value of T_c of the top electrode.

In Figure 3, we present an example of IV characteristics at selected applied magnetic fields for a ramp-edge junction made of PCCO x = 0.15 superconducting electrodes on STO at 4.2K. In this particular case, the normal resistance of the junction, evaluated as the slope of the IV curve at high current, is roughly 0.5 Ω : in most cases, this resistance can vary from 50 mΩ to 1 Ω . Using a voltage criterion of 1 μV, one can extract from these IV curves the field dependence of the critical current. An example is shown in the inset of Fig. 3 for a similar junction at 9K. The field dependence reveals the presence of strong variations at periodic interval of magnetic field indicating the penetration of magnetic flux in a quantized fashion. This behaviour is that expected of Josephson junctions with well-defined phase difference across the barrier. We should note however that critical current oscillations are not following the expected Fraunhöfer-like pattern for small junctions. Because of our crude definition of bridges with the diamond scriber leading to fairly large junctions and the fact that the critical current density in our junctions can be as large as 10000 A/cm^2, one remains in the large junction limit [1]. This results in non-uniform flux penetration and current density distribution in the junctions [9]. Nevertheless, we obtain junctions for which the maximum critical current densities compare well with those made with hole-doped cuprates [6].

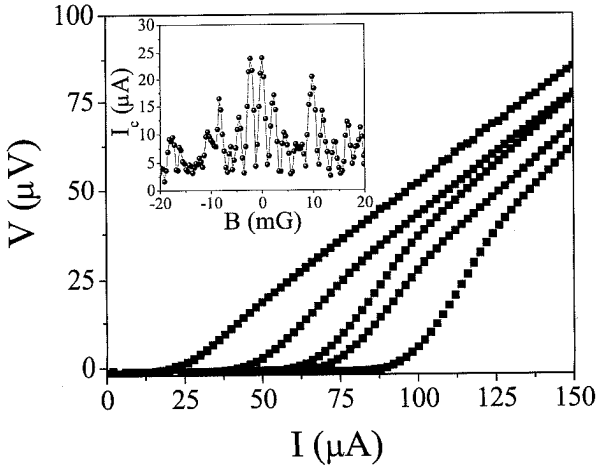

Fig. 3 Current-voltage (IV) curves for a few selected applied magnetic fields at 4.2K for a junction made with PCCO x = 0.15 electrodes and x = 0.05 barrier on a $SrTiO_3$ substrate. The barrier thickness along the current direction is 38nm and the width of the junction is approximately 100 μm. Inset : magnetic field dependence of the critical current of a similar junction at 9K.

As another test of the quality of these junctions, one can expose them to external RF fields. In Figure 4, we present an IV curve of a junction on LSAT at zero magnetic field and in a RF field of ν = 20 GHz. At the appropriate power level, we observe the expected Shapiro steps at regular interval of voltages. Using the derivative of this IV characteristic, one can better pinpoint the voltage position of these steps. For this particular example, we can observe well-defined steps at an interval of $\Delta V \sim 40$ μV in close agreement with the expected theoretical value of $\Delta V_{SC} = h\nu/2e$ [1,9]. Moreover, one can observe anomalies (marked by stars in Fig. 4) corresponding to photon-assisted quasi-particle tunnelling at half the voltage interval of the regular Shapiro steps, i.e. at $\Delta V_{QP} = \Delta V_{SC} / 2$ once again as expected theoretically [1,9]. Overall, the observation of Shapiro steps following qualitatively the theoretical expectations in these junctions is a good indication of well-defined phase differences between the electrodes. Together with the magnetic field dependence of the critical current, they are indicating well-behaved junctions.

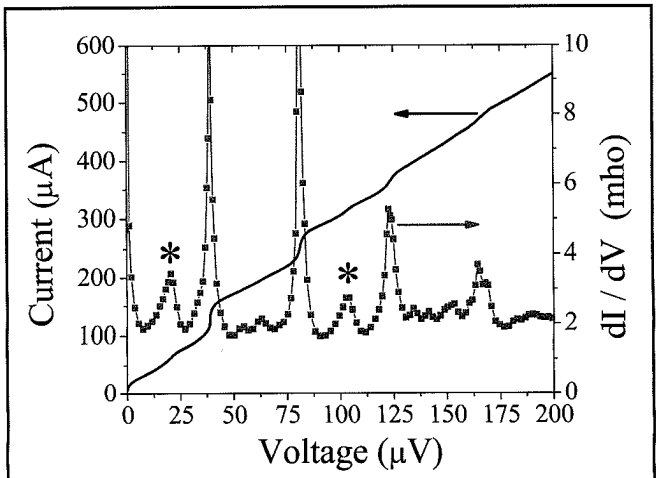

Fig. 4 IV curve (solid black line) at 4.2K and zero magnetic field in an ambient RF field of 20GHz showing Shapiro steps. Grey squares and solid line: derivative dI/dV pinpointing to the Shapiro steps but also to the photon-assisted quasi-particle tunnelling signatures indicated by stars.

In a more complete study presented elsewhere [7], we explored also the temperature dependence of the critical current density ($J_c = I_c/A$ where A is the cross-sectional area of the junction) at zero magnetic field. Its $J_c = J_{co}(T - T_c)^2$ dependence from $T = 0.4\ T_c$ to T_c is very similar to that of other reported ramp-edge Josephson junctions based on hole-doped cuprates [6] and is in close agreement with the expectation from the proximity effect theory [10,11]. The lack of irreversibility in the IV curves and this temperature dependence of J_c are clear signatures of superconducting-normal-superconducting (SNS) junctions.

These SNS junctions could in fact be used to explore the coupling through a wide variety of barriers. By varying the barrier thickness for example, the coherence length of the superconducting pairs within the metallic barrier can be extracted and compared to theoretical predictions. In our case, the choice of a PCCO x = 0.05 barrier was motivated by our worries regarding the difficult growth conditions and the likely positive impact of interface reconstruction. Moreover, since PCCO x = 0.05 is an antiferromagnet at temperatures used in our junctions [12], it is interesting to see that the magnetic phase does not prevent the coupling between the superconducting electrodes. It suggests exploring more thoroughly the barrier doping dependence of this coupling through proximity effect. Finally, it would be also interesting to investigate any potential impact of the doping of the superconducting electrodes on the coupling.

ACKNOWLEDGEMENTS

We thank M. Poirier, D. Stornaiuolo, F. Tafuri and S. Charlebois for fruitful discussions and K.D. Truong, S. Pelletier, M. Lacerte and M. Castonguay for technical assistance. We acknowledge the support of CFI, NSERC (Canada), FQRNT (Québec) and the Université de Sherbrooke.

REFERENCES

1. M. Tinkham, *Introduction to superconductivity*, second edition, McGraw-Hill, Inc., New York, (1996).
2. John Clarke and Alex I. Braginski, *The SQUID Handbook: Fundamentals and Technology of SQUIDs and SQUID Systems*, Wiley-VCH, Berlin, (2006).
3. R.C. Black, A. Mathai, F.C. Wellstood, E. Dantsker, A.H. Miklich, D.T. Nemeth, J.J. Kingston and J. Clarke, *Appl. Phys. Lett.* **62**, 2128 (1993).
4. D.J. Van Harlingen, *Rev. Mod. Phys.* **67**, 515 (1995).
5. C.C. Tsuei and J.R. Kirtley, *Rev. Mod. Phys.* **72**, 969 (2000).
6. F. Tafuri and J.R. Kirtley, *Rep. Prog. Phys.* **68**, 2573 (2005).
7. G. Roberge, S. Charpentier, S. Godin-Proulx, and P. Fournier, *J. Appl. Phys.*, **109**, 073912 (2011).
8. G. Roberge, S. Charpentier, S. Godin-Proulx, P. Rauwel, K. Truong, and P. Fournier, *J. Crystal Growth* **311**, 1340 (2009).
9. A. Barone and G. Paternò, *Physics and Applications of the Josephson Effect*, John Wiley & Sons, Inc., New York, (1982).
10. P.G. de Gennes, *Rev. Mod. Phys.* **36**, 225 (1964).
11. K.A. Delin and A.W. Kleinsasser, *Supercond. Sci. and Tech.* **9**, 227 (1996).
12. N.P. Armitage, P. Fournier and R.L. Greene, *Rev. Mod. Phys.* **82**, 2421 (2010).

... Continued from page 118 (Electrostatic Gating ... by A.D. Caviglia *et al.*)

22. A. Brinkman, M. Huijben, M. van Zalk, J. Huijben, U. Zeitler, J.C. Maan, W.G. van der Wiel, G. Rijnders, D.H.A. Blank, and H. Hilgenkamp, *Nat Mater* **6** (7), 493-496 (2007).
23. A.D Caviglia, M. Gabay, S. Gariglio, N. Reyren, C. Cancellieri, and J.-M. Triscone, *Phys. Rev. Lett.* **104** (12), 126803 Mar (2010).
24. M. Ben Shalom, M. Sachs, D. Rakhmilevitch, A. Palevski, and Y. Dagan, *Phys. Rev. Lett.* **104** (12), 126802 Mar (2010).
25. A.D. Caviglia, S. Gariglio, C. Cancellieri, B. Sacépé, A. Fête, N. Reyren, M. Gabay, A.F. Morpurgo, and J.-M. Triscone, *Phys. Rev. Lett.* **105** (23), 236802 Dec (2010).